Two High-Resolution Crystal Structures of the Recombinant N-Lobe of Human Transferrin Reveal a Structural Change Implicated in Iron Release[†,‡]

Ross T. A. MacGillivray,*[,§] Stanley A. Moore,[||] Jie Chen,[§,⊥] Bryan F. Anderson,[||] Heather Baker,[||,#] Yaoguang Luo,[§] Maria Bewley,[||,$] Clyde A. Smith,[||,#] Michael E. P. Murphy,[§] Yili Wang,[§] Anne B. Mason,[@] Robert C. Woodworth,[@] Gary D. Brayer,[§] and Edward N. Baker[||,#]

Department of Biochemistry and Molecular Biology, University of British Columbia, Vancouver, British Columbia V6T 1Z3, Canada, Institute of Molecular Biosciences, College of Sciences, Massey University, Private Bag 11222, Palmerston North, New Zealand, and Department of Biochemistry, University of Vermont, Burlington, Vermont 05405-0068

Received February 13, 1998

ABSTRACT: The N-lobe of human serum transferrin (hTF/2N) has been expressed in baby hamster kidney cells and crystallized in both orthorhombic ($P2_12_12_1$) and tetragonal ($P4_12_12$) space groups. Both crystal forms diffract to high resolution (1.6 and 1.8 Å, respectively) and have been solved by molecular replacement. Subsequent refinement resulted in final models for the structure of hTF/2N that had crystallographic *R*-factors of 18.1 and 19.7% for the two crystal forms, respectively; these models represent the highest-resolution transferrin structures determined to date. The hTF/2N polypeptide has a folding pattern similar to those of other transferrins, including the presence of a deep cleft that contains the metal-binding site. In contrast to other transferrins, both crystal forms of hTF/2N display disorder at the iron-binding site; model building suggests that this disorder consists of alternative conformations of the synergistically bound carbonate anion, the side chain for Arg-124, and several solvent molecules. Subsequent refinement revealed that conformation A has an occupancy of 0.63−0.65 and corresponds to the structure of the iron-binding site found in other transferrins. The alternative conformation B has an occupancy of 0.35−0.37; in this structure, the carbonate has rotated 30° relative to the iron and the side chain for Arg-124 has moved to accommodate the new carbonate position. Several water molecules appear to stabilize the carbonate anion in the two conformations. These structures are consistent with the protonation of the carbonate and resulting partial removal of the anion from the metal; these events would occur prior to cleft opening and metal release.

The transferrins are a group of bilobal proteins that contain two homologous metal-binding sites with high affinities for ferric iron (*1*). Although originally thought to be restricted to vertebrates, transferrin-like proteins have now been identified in several invertebrate species where they occur in the hemolymph (*2*). In vertebrates, the transferrins are found in a variety of bodily fluids, including the serum transferrins found in blood, the ovotransferrins found in avian egg white, the lactoferrins found in milk, tears, saliva, and other secretions, and the melanotransferrins found anchored to the membrane surfaces of melanocytes and other cells via a glycosyl−phosphatidylinositol linkage. Each of these vertebrate transferrins consists of a single polypeptide chain with an M_r of ∼80000 containing two structurally similar binding sites for ferric iron and other metals; on binding ferric iron and a synergistic anion, these proteins display typical absorption spectra with absorption maxima around 465 nm.

Determination of the amino acid sequence of human transferrin (hTF[1]) revealed extensive sequence identity between the amino- and carboxyl-terminal halves of the polypeptide chain (*3*). This sequence homology has been found in other transferrins such as rabbit transferrin, human lactoferrin, and hen ovotransferrin (*4*, *5*). These data suggest

[†] Supported by grants from the U.S. Public Health Service (R01 DK 21739 to R.C.W. and R01 HD 20859 to E.N.B.), the Medical Research Council of Canada (to G.D.B.), and the Protein Engineering Network Center of Excellence (to G.D.B.). During his stay at Massey University, R.T.A.M. was supported in part by a Killam Senior Research Fellowship and by U.S. Public Health Service Grant R01 DK 35533. E.N.B also acknowledges research support as an International Research Scholar of the Howard Hughes Medical Institute.

[‡] Atomic coordinates of the protein structures reported in this paper have been deposited with the Protein Data Bank at Brookhaven National Laboratories with PDB codes 1A8E and 1A8F for the orthorhombic and tetragonal crystal forms, respectively.

* Corresponding author. Telephone: (604) 822-3027. Fax: (604) 822-4364. E-mail: macg@unixg.ubc.ca.

[§] University of British Columbia.

[||] Massey University.

[⊥] Current address: Institute of Molecular Biophysics, Florida State University, Tallahassee, FL 32308.

[#] Current address: School of Biological Sciences, University of Auckland, Private Bag 92019, Auckland, New Zealand.

[$] Current address: Brookhaven National Laboratory, Upton, NY 11973-5000.

[@] University of Vermont.

[1] Abbreviations: hTF, human serum transferrin; hTF/2N, recombinant N-lobe of human transferrin comprising residues 1−337; hTF/2C, recombinant C-lobe of human transferrin comprising residues 338−681; hLF, human lactoferrin; hLF/2N, recombinant N-lobe of human lactoferrin; BHK cells, baby hamster kidney cells; NTA, nitrilotriacetate; EDTA, ethylenediaminetetraacetic acid; RMS, root-mean-square; CRB, carbonate.

S0006-2960(98)00355-9 CCC: $15.00
Published on Web 05/12/1998

Table 1: Transferrin Structures

protein	source	pH	resolution (Å)	ref
human $(Fe)_2$−LF	milk	7.8	2.2	*9*
bovine $(Fe)_2$−LF	milk	7.7	2.8	*14*
human Fe−LF/2N	BHK cells	8.0	2.0	*55*
human $(Cu)_2$−LF	milk	7.8	2.1	*54*
human apo-LF	milk	8.2	2.8	*15*
chicken (Fe)−ovoTF/2N	egg white	5.9	2.3	*31*
chicken $(Fe)_2$−ovoTF	egg white	5.9	2.4	*11*
duck $(Fe)_2$−ovoTF	egg white	5.8	2.35	*12*
duck Fe−ovoTF/4N (domain 2)	egg white	7.8	2.3	*13*
duck apo-TF	egg white	6.0	4.0	*16*
rabbit $(Fe)_2$−TF	serum	6.0	3.3	*10*
human Fe−TF	serum	5.75	2.6	*51*
human Fe−TF/2N	BHK cells	5.75	1.6	this study
human Fe−TF/2N	BHK cells	6.1	1.8	this study

that the modern day transferrins have evolved by means of a gene duplication event from an ancestral gene coding for a protein with an M_r of ∼40000 containing a single metal-binding site. Subsequent duplications of this larger gene have given rise to the transferrins, lactoferrins, and melanotransferrins found today. The organization of the human transferrin gene is consistent with this evolutionary history (*6*).

Crystallographic studies of human lactoferrin gave the first detailed view of transferrin three-dimensional structure (*7*, *8*). This structure, subsequently refined to 2.2 Å resolution (*9*), showed that the polypeptide is folded into two homologous lobes (referred to as the N-lobe and C-lobe) representing the N- and C-terminal halves of the molecule. The two lobes are joined by a connecting peptide which in lactoferrin forms a three-turn α-helix. Each lobe is further subdivided into two similar α/β domains separated by a deep cleft that contains the binding site for ferric iron; in each lobe, the ligands to iron are the same: two tyrosine residues, a histidine residue, and an aspartic acid residue together with two oxygen atoms of a bidentate carbonate ion that is bound synergistically with iron. Subsequent crystallographic analyses have led to the determination of the three-dimensional structures of other transferrin molecules. These are listed in Table 1 and include the diferric forms of rabbit transferrin (*10*), chicken ovotransferrin (*11*), duck ovotransferrin (*12*) and an 18 kDa iron-binding fragment of duck ovotransferrin (*13*), and bovine lactoferrin (*14*), as well as various fragments, mutants, and metal- and anion-substituted proteins (Table 1). Although there are some subtle differences, the folding and iron-binding sites of all these species are essentially similar to those originally described for lactoferrin (*1*).

The structural changes that accompany iron binding and release have also been defined by crystallographic studies of human apolactoferrin (*15*) and, at lower resolution, duck apoovotransferrin (*16*) (see Table 1). Light scattering studies of solutions further show that all transferrins undergo similar structural changes (*17*). Iron binding or release is associated with a large-scale domain movement that results in closing or opening of the binding cleft of each lobe. This conformational change is mediated by a hinge in the two antiparallel β-strands that run behind the iron-binding site in each lobe; in the N-lobe of human lactoferrin, for example, one domain rotates by 54° relative to the other about this hinge (*15*).

Despite these recent developments in the understanding of the structural changes that accompany metal binding to the transferrin family of molecules, the actual mechanisms of iron binding and release in vivo are still unclear. It is now known that serum transferrin binds to its cellular receptor and the resulting complex is internalized by endocytosis (*18*). Once the complex is inside the cell, intravesicular acidification leads to a lowering of the pH within the endosome with the release of iron from transferrin occurring below pH 6. While the subsequent transport of the released iron within the cell is still unclear, it has been shown that the transferrin−transferrin receptor complex is recycled to the plasma membrane where both are reused (*19*). In addition to these studies in cell lines, the release of iron from human transferrin has been studied extensively using purified proteins. Initial studies with anions such as oxalate or malonate at the anion-binding site of transferrin showed that these anions inhibited iron acquisition by reticulocytes but did not prevent binding of the transferrin to the receptor, suggesting the involvement of the carbonate in iron release (*20*−*23*). These and subsequent studies have implicated carbonate protonation (*24*−*27*) and the transferrin receptor (*28*−*30*) in the release mechanism.

A possible explanation for the pH dependence of iron release (and for differences between different iron-binding sites) has been advanced by Dewan and colleagues following examination of the crystal structure of the ferric ovotransferrin N-lobe (*31*). Two lysine residues (Lys-206 and Lys-296 using the hTF/2N numbering[2]) appeared to be too close to each other for both to be protonated within the molecule. As these two lysine residues are found in the N1 and N2 domains, respectively, and appear on opposite faces of the cleft near the iron-binding site, Dewan et al. suggested that they comprise a pH-sensitive dilysine trigger. If one of the lysine residues had an abnormally low pK_a (below the normal pK_a of ∼10 for the ϵ-amino group), then at pH 5.9 (the pH at which the ovotransferrin crystal structure was determined) one of the lysine residues would not be positively charged. Upon further reduction of the pH, the NZ amino group of this lysine residue would become protonated and the two charged lysine residues would repel each other, providing an electrostatic force for opening the cleft containing the iron-binding ligands. The dilysine trigger is an attractive hypothesis for explaining the more facile iron release observed from the N-lobe of transferrins relative to the release from their C-lobes and relative to the release from the human and mouse lactoferrins (which have amino acid substitutions that disrupt the proposed triggers). However, bovine lactoferrin appears to be anomalous as it has an N-lobe of the serum transferrin type (Lys-Lys), yet it is otherwise a typical lactoferrin in that Lys-301 (hLF numbering) makes a salt bridge with Glu-216 and Lys-210 NZ occupies the same position as Arg-210 NH1 in hLF (*14*). Hence, the NZ atoms in question do not make the close contact in bovine lactoferrin that is found in hTF.

In this paper, we describe two high-resolution crystal structures for the iron-bound, recombinant N-lobe of human serum transferrin. These structures were obtained from the protein crystallized in two different space groups and

[2] Except where noted in the text, all amino acid numbering is taken from the human transferrin sequence (*38*).

Table 2: Data Collection Statistics of hTF/2N Crystallized in Two Different Space Groups

	crystal form I	crystal form II
space group	$P2_12_12_1$	$P4_12_12$
cell dimensions (Å)	$a = 45.12$, $b = 57.91$, $c = 135.64$	$a = b = 72.67$, $c = 154.29$
resolution (Å)	1.6	1.8
R_{merge} on I	0.061	0.082
$\langle I\rangle/\langle\sigma(I)\rangle$	14.6	6.6
completeness (%)	82.4	94.0
unique reflections	39 418	36 895
redundancy	1.8	4.8

represent the highest-resolution transferrin structures to date (at 1.6 and 1.8 Å resolution). Both hTF/2N structures show overall folding patterns similar to those of other transferrin and lactoferrin N-lobe structures determined to date. However, both hTF/2N structures reveal alternative conformations of the synergistically bound carbonate anion and the side chain for Arg-124. In contrast, the electron density maps show no disorder and very low crystallographic *B*-factors for the side chain atoms of Lys-206 and Lys-296. These data suggest that protonation of the anion with concomitant movement of the anion and side chain of Arg-124 may comprise the initial step in the pH-induced release of iron from transferrin; this localized conformational change appears to precede any structural movement of the residues that comprise the suggested dilysine trigger.

EXPERIMENTAL PROCEDURES

Materials. All chemicals were reagent grade or better.

Recombinant Protein Production. Recombinant hTF/2N was expressed using the pNUT-BHK cell system as described previously (*32*). After saturation with Fe(III)−NTA, the hTF/2N was purified from the tissue culture medium using modifications that have been described in detail (*33*). The purity of the hTF/2N was assessed by polyacrylamide gel electrophoresis in the presence of SDS and electrospray mass spectroscopy (*34*).

Crystallization of Recombinant hTF/2N. *Crystal Form I (Space Group $P2_12_12_1$).* Initially, hTF/2N was crystallized by using the hanging drop method as described previously (*35*). The protein was crystallized at 4 °C from a solution of 40 mM sodium cacodylate buffer (pH 5.75) containing 20 mM sodium bicarbonate and 26% polyethylene glycol 4000. After 7−30 days, large deep red crystals appeared with dimensions of 1.8 mm × 0.8 mm × 0.4 mm (see Table 2).

Crystal Form II (Space Group $P4_12_12$). A second crystal form for hTF/2N was obtained by using ethanol as a precipitant. Ferric-saturated hTF/2N was dissolved and dialyzed against 20 mM sodium bicarbonate (pH 8.1) and concentrated to ∼80 mg/mL using a Centricon 10 Microconcentrator. Crystals were obtained at 4 °C by using the sitting drop method in microbridges. The drop contained 1.5 μL of 50 mM potassium cacodylate buffer (pH 6.1) containing 40% (v/v) ethanol. The reservoir contained 40% (v/v) ethanol in 50 mM potassium cacodylate buffer in the pH range of 5.9−6.3. After 7−30 days, large deep red, tetragonal prisms appeared with dimensions of 1.25 mm × 1.0 mm × 0.5 mm. The crystals belonged to the tetragonal space group $P4_12_12$ (Table 2). Prior to data collection, the crystals were transferred to a cryogenic mother liquor containing 40% (v/v) 2-methyl-2,4-pentanediol.

Table 3: Refinement Statistics of hTF/2N for Two Different Space Groups

	crystal form I ($P2_12_12_1$)	crystal form II ($P4_12_12$)
resolution range (Å)	30.0−1.60	32.0−1.80
molecules in asymmetric unit	1	1
working *R*-factor	0.181	0.197
free *R*-factor	not used	0.253
rms deviation from ideal geometry		
bond length (Å)	0.013	0.012
bond angles (deg)	1.60	1.60
average *B*-factor (main chain) (Å^2)	31.3	22.5
average *B*-factor (side chains) (Å^2)	40.7	26.9
average *B*-factor of solvent (Å^2)	28.8	31.6
number of non-H atoms	2714	2846
protein atoms (including alternative conformations of some residues)	2568	2570
Fe(III) + CRB (two conformations)	9	9
number of solvent atoms	137	267

Data Collection. Data were collected using a Rigaku R-Axis IIc image plate detector on a Rigaku RU300 or RTP 300 rotating anode generator operated at 50 kV and 100 mA. For the form I crystal, data were collected at 7 °C from a single crystal. For form II crystals, data were collected at 113 K using an Oxford Cryosystems cooling unit. The data collection statistics for both crystal forms are given in Table 2. Crystal form I data were processed using the software supplied with the R-Axis detector system, while diffraction images for crystal form II were processed using the program DENZO (*36*) and subsequently scaled and merged using the programs ROTAVATA and AGROVATA in the CCP4 suite of programs (*37*).

Structure Solution and Refinement. *Crystal Form I (Space Group $P2_12_12_1$).* The structure was solved by molecular replacement using as a search model the coordinates of rabbit transferrin (*10*) in which appropriate amino acid side chain substitutions had been made to reflect the amino acid sequence of human transferrin (*38*). A single clear solution was obtained with an initial *R*-factor of 45% for all data between 8 and 2.8 Å resolution. Molecular dynamics refinement using XPLOR (*39*) punctuated with rounds of manual rebuilding with TOM reduced the *R*-factor to 18.1% using the data from 8 to 1.6 Å resolution. Water molecules were added and were allowed to refine freely. Subsequent restrained least-squares refinement using the program TNT (*40*, *41*) led to reinterpretation of the positioning of the carbonate anion and the introduction of alternative conformations for this and for the side chains of several residues, including Arg-124. Residues Pro-142 and Pro-145 were also modeled in the cis conformation; the resulting structure was more consistent with the observed electron density and resulted in lower temperature factors for these residues. Residues 1, 2, and 332−337 of hTF/2N are disordered and are not present in the final model. The final refinement statistics of the model are shown in Table 3.

Crystal Form II (Space Group $P4_12_12$). The structure was solved by molecular replacement using the program AMoRe (*42*). The protein coordinates of a partially refined structure of crystal form I were used as the search model. The best translation function solution was in space group $P4_12_12$ and

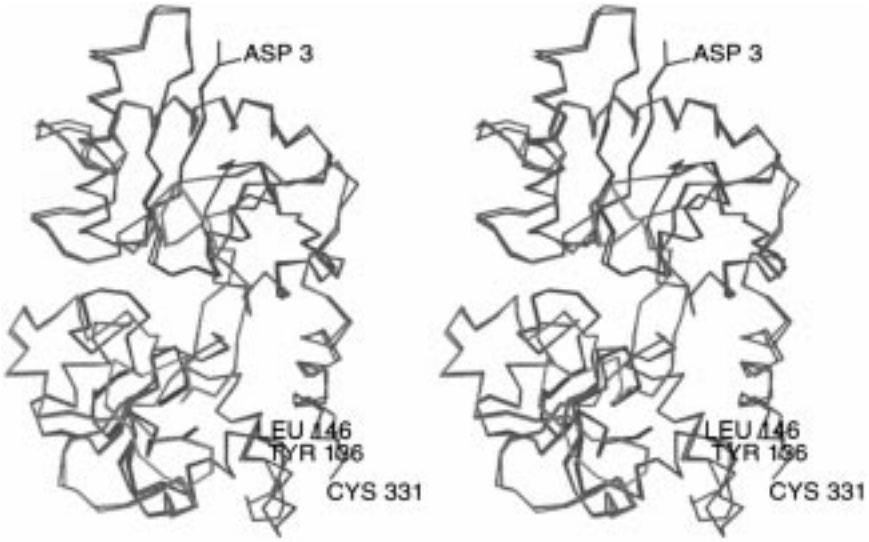

FIGURE 1: Comparison of the structures of hTF/2N in two different crystal forms. Stereo representations of the α-carbon backbones of the molecules are shown for the orthorhombic crystal form (red) and the tetragonal crystal form (green). The structures were superimposed using the program XtalView (*56*); the cleft containing the iron-binding site is at the center left of the molecules. The N termini (Asp-3), C termini (Cys-331), and the variable loop (Tyr-136−Leu-146) are labeled.

gave a correlation coefficient of 0.578 and an *R*-factor of 0.397 for all data between 8.0 and 4.0 Å resolution. The best translation function solution in the enantiomorphic space group ($P4_32_12$) gave a much less convincing result (correlation coefficient = 0.318, *R*-factor = 0.487); hence, the correct space group was $P4_12_12$. Rigid body refinement using the program AMoRe (*42*) resulted in a linear correlation coefficient of 0.63 and an *R*-factor of 0.360. Again, the structure was refined using the program TNT; initially, the atoms comprising the metal-binding site [the side chains of ligands Asp-63, Tyr-95, Arg-124, Tyr-188, and His-249, the carbonate anion, and the Fe(III) ion] were deleted from the model and were rebuilt into $2F_o - F_c$ and $F_o - F_c$ difference electron density maps.

Water molecules were built into the maps in places where (i) the electron density was spherical, (ii) the water molecules were able to form at least one hydrogen bond with the polypeptide chain and/or another water molecule, and (iii) there was at least a 3.0σ peak in the SIGMAA weighted $F_o - F_c$ difference Fourier synthesis (*43*). In subsequent rounds of refinement, water molecules were deleted if their *B* values were greater than 60 Å^2. In the rare instances when water molecules had high *B* values but formed strong hydrogen bonding networks with other atoms in the model, the occupancies were adjusted to 0.50. The final rounds of refinement involved the modeling of several side chains in alternative conformations and, in particular, the modeling of the side chain of Arg-124, the carbonate anion, and associated water molecules. Finally, the two alternative binding configurations of the carbonate were refined using SHELXL (*44*). The first configuration, which corresponds to that found in Fe(III)−lactoferrin and other transferrins (see Table 1), comprises the carbonate and side chain of Arg-124 (both in conformation A) and water molecules WAT-700, -701, and -702. Configuration B comprises alternative conformations for the carbonate and Arg-124 side chain and WAT-699. *X*, *Y*, *Z*, and *B* values for all atoms were allowed to vary, but the occupancies of configuration A were constrained to be the same as those of configuration B; the sum of these two occupancies was constrained to equal unity. After refinement, configuration A had an occupancy of 0.65 and configuration B 0.35. Residues 1, 2, and 332−337 were disordered and are not present in the final model. The final refinement statistics for the crystal form II data are given in Table 3.

RESULTS AND DISCUSSION

Crystallization of hTF/2N. Depending on the conditions, the recombinant N-lobe of human transferrin crystallized in two different crystal forms that both diffract to high resolution (to 1.6 and 1.8 Å, respectively). This probably reflects the homogeneity of the recombinant protein since it has been observed previously that recombinant hTF/2N is more monodisperse than the half-molecule derived proteolytically from serum transferrin (*32*). As both glycosylation sites are present in the C-lobe of hTF (*3*), the isolated hTF/2N is not glycosylated (*32*), thereby eliminating the heterogeneity in glycosylation that is observed with both serum-derived and recombinant full-length transferrins (which include a glycosylated C-lobe) (*45*).

Polypeptide Folding of Fe(III)−hTF/2N. In both crystal forms, the overall folding of the molecule is essentially the same (Figure 1) and is also very similar to that of the iron-loaded N-lobes of other transferrins and lactoferrins. The polypeptide is folded into two globular domains separated by a deep cleft in which the iron-binding site is located. Using the terminology first adopted for lactoferrin (*1*, *7*), the N1 domain comprises residues 1−93 and 247−315 and the N2 domain consists of residues 94−246. Both domains have a similar α/β fold in which a number of helices are packed against a central mixed β-sheet. The domains are connected by two extended β-strands running antiparallel to each other; in lactoferrin, these two β-strands form the hinge that allows the domains to close and open on metal binding and release, respectively. The iron-binding ligands are contributed by the N1 domain (Asp-63), the N2 domain (Tyr-188), and the two interdomain β-strands (Tyr-95 and His-249). The side chain of Arg-124 from the N2 domain also plays a key role in binding the essential carbonate ion (see below).

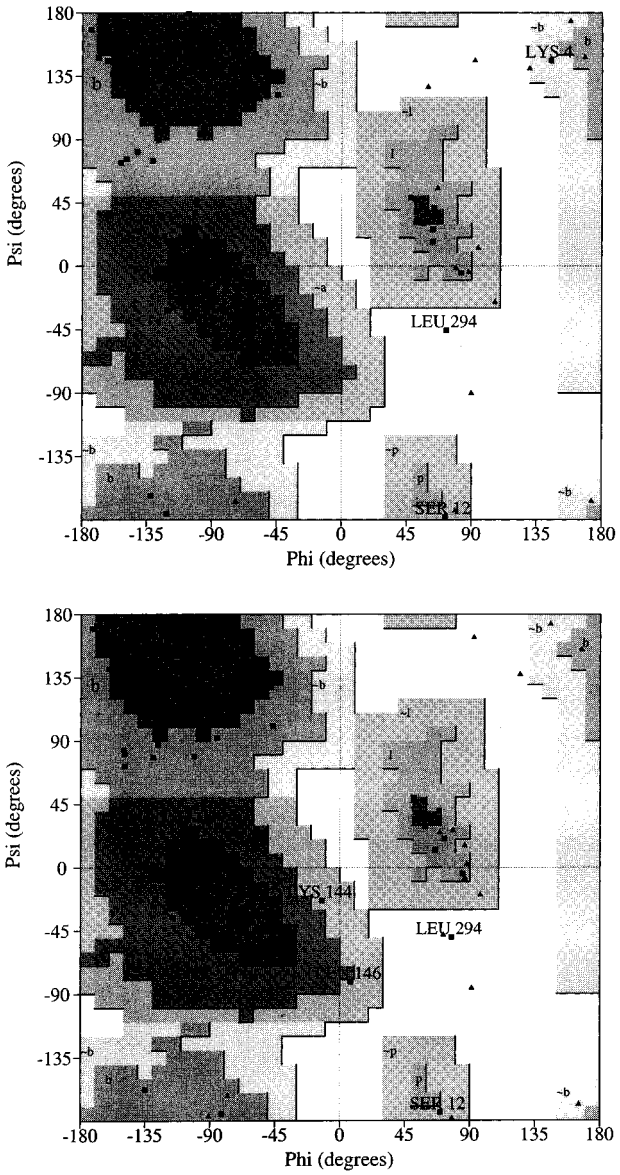

FIGURE 2: Distribution of main chain torsion angles for hTF/2N in two different crystal forms: (A) orthorhombic crystal form and (B) tetragonal crystal form. Glycine residues are shown as triangles and non-glycine residues as squares. The apparent conformational variations of Leu-294 are labeled. The plots were generated by using the program PROCHECK (*57*).

Ramachandran plots (*46*) of the main chain torsion angles of hTF/2N in each crystal form are presented in Figure 2. Only one residue (Leu-294) falls outside the permissible regions; this residue has ϕ and φ angles of 73 and $-45°$, respectively, and allows a tight turn that has the conformation of a reverse classical γ-turn (*47*) so that the carbonyl group of Leu-293 forms a hydrogen bond with the amino nitrogen of Phe-295. Additional hydrogen bonds involving Leu-293 (between Leu-293 O and the NZ of Lys-18 and between Leu-293 N and the OE2 of Glu-15) contribute to the stability of this unusual structural feature. This γ-turn, which forms part of one wall of the binding cleft, has also been found in the N- and C-lobes of all the other transferrin crystal structures determined to date (Table 1). The three residues, Leu-Leu-Phe, that form the γ-turn are conserved in both lobes of all mammalian and avian transferrins whose amino acid sequences have been determined (*5*), suggesting that this γ-turn is highly conserved among all transferrins.

The distribution of temperature factors follows the same pattern for the molecules in both crystal forms, reflecting the relative rigidity of different parts of the molecules. Temperature factors are lowest for those residues involved in liganding to the iron (residues 63, 95, 188, and 249), internal residues, and those that form the walls of the iron-binding cleft. The three longest continuous segments of polypeptide with lower than average temperature factors are comprised of residues 116−123, 170−212, and 279−307 (this includes the γ-turn consisting of residues 293−295) which all contribute to the formation of the binding cleft. Regions with higher than average temperature factors include residues 29−34, 71−74, 87−90, 103−113, 136−145, 165−168, 215−218, 277, and 278, and all represent surface loops in hTF/2N. Similar high temperature factor profiles have been noted for these regions in the other transferrins whose crystal structures have been determined (*9*, *10*). With the exception of the disulfide bridge between Cys-137 and Cys-331, all of the cysteinyl residues have low temperature factor values and appear to form stable disulfide bridges in the structures. The increased thermal motion of Cys-331 may reflect its position close to the interlobe connecting peptide which is disordered in both crystal forms; in the full-length transferrin molecule, the C-lobe would be expected to exert some constraints on this bridge region. The lower average *B*-factor of the tetragonal crystal form, compared to that of the orthorhombic form (Table 3), probably reflects the lower temperature of data collection (117 K compared to 7 °C).

Differences between the Two Crystal Forms of hTF/2N. As shown in Figure 1, the major difference between the orthorhombic and tetragonal crystal forms of hTF/2N occurs at a surface loop between residues 136 and 145. This loop forms a crystal contact in the tetragonal form but not in the orthorhombic form; in the tetragonal form, the loop contacts the equivalent loop in a symmetry-related molecule and has poorly defined electron density for much of its course, implying considerable disorder for this region of polypeptide chain. Other less extensive conformational differences are at the amino terminus (residues 3 and 4), the 307−308 peptide bond (which appears to be flipped between the two forms), and the 106−107 peptide bond (rotated 90° in the tetragonal crystal to accommodate stacking with an arginine side chain). Last, the loop of residues 255−257 is well ordered in the orthorhombic crystal and makes a lattice contact with the C-terminal helix of a neighboring molecule, whereas this loop is disordered and makes no contacts in the tetragonal crystal.

Within the two crystals, the segment from residue 316 to 328 appears to be related largely by a rigid body movement together with some side chain conformational differences. However, many of the side chains in this region are poorly defined in the electron density maps. The carboxyl-terminal region (residues 329−331) also has weak electron density but appears to have different conformations in the two crystal forms. Other minor differences between the two crystal forms of hTF/2N are listed in Table 4. Most of these differences reflect intermolecular crystal contacts that are unique in the two crystal forms; the presence of a crystal contact results in the stabilization of a side chain in one crystal form, while the absence of the crystal contact results in a disordered side chain in the other crystal form. A number of amino acid side chains also exhibit multiple

Table 4: Differences between the Orthogonal and Tetragonal Crystal Forms of hTF/2N

residue	orthorhombic form	tetragonal form
Gln-20	no contacts, weak density	crystal contact with Gln-111, reasonable density
Glu-56	crystal contact, reasonable density	no contact, poor density
Tyr-71	no interaction with Lys-312	interacts with Lys-312
Gly-106	no crystal contact	crystal contact with Arg-23 requires peptide rotation of 90° to accommodate stacking interaction
Met-109	CE atom in a different place in the two crystal forms	
Gln-111	no crystal contact, relatively weak density	crystal contact, good density
Arg-113	interaction with the loop of residue 138, relatively weak density	good density, no contacts
Leu-122	χ_2 different in two forms	
Pro-145	cis peptide	trans peptide
Asp-166	weak density, no contact	good density, near contact
Leu-182	side chains different in the two structures	
Gln-245	crystal contacts, relatively weak density	weak density, no contact
Asp-261	crystal contact, plus water contact	weak density, no contact
Leu-262	side chains different, relatively weak density	
Met-256	good density, crystal contact	weak density, residues 255−257 disordered
Glu-265	different side chain position	position of Glu-265 side chain in contact with Arg-324, Tyr-317 in orthorhombic structure
Glu-272	relatively weak density, crystal contact	weak density, no contact
His-273	good density in both, different χ_2 angles, ring flipped 180° for hydrogen bonding potential	
Glu-281	relatively good density, crystal contacts	weak density, no crystal contacts
Pro-307	peptide flip and Arg-308	
Arg-308	in different orientation	
Met-313	weak density, different side chain position	excellent density, crystal contact

conformations in the two crystal forms; multiple conformers of residues Ser-44, Arg-124, Ser-248, Thr-250, and Ser-255 are found in the orthorhombic form, and multiple conformers of Ser-21, Met-26, Asn-76, Arg-124, and Ser-248 are found in the tetragonal form. In addition, alternative forms of the carbonate are found in both crystal forms (see below).

Structural Comparison with Other Transferrins. As summarized in Table 1, the three-dimensional structures of several iron-loaded transferrins have been determined, including those of rabbit serum transferrin (at 3.3 Å resolution), chicken ovotransferrin (2.4 Å), human lactoferrin (2.2 Å), and bovine lactoferrin (2.8 Å). The α-carbons of these structures were superimposed on each other by using the programs POLYPOSE (*48*) and Clusterid (*49*). As expected, hTF/2N shows the greatest structural similarity to the N-lobe of rabbit transferrin (rms difference between α-carbons = 0.62 Å), followed by the N-lobes of ovotransferrin and human lactoferrin (rms differences = 0.82 and 1.04 Å, respectively). The structure most different from hTF/2N is the C-lobe of rabbit transferrin (rms difference = 1.17 Å). These structural similarities reflect the polypeptide folding patterns which are more or less identical in the transferrins, and which give rise to the cleft containing the iron-binding site (involving ligands from amino acids that are located throughout the polypeptide chain). As suggested by amino acid sequence comparisons (*5*), the major structural differences between the N-lobes of the transferrins and lactoferrin are variations in the sequences and sizes of surface loops; these differences probably account in part for the species specificity in the binding of transferrins to their receptors (*50*).

Alternative Conformations at the Iron-Binding Site of hTF/2N. In all iron-bound transferrins whose structures have been determined to date, the ligands to the Fe(III) ion consist of the side chains of two tyrosyl residues, an aspartic acid residue, a histidine residue, and the carbonate anion; in hTF/2N, these liganding side chains are contributed by Asp-63, Tyr-95, Tyr-188, and His-249. During the refinement of the orthorhombic crystal form of hTF/2N, strong electron density was observed around the bound Fe(III). The side chains of Asp-63, Tyr-95, Tyr-188, and His-249 were built into this density and corresponded approximately to the positions of these side chains in the other transferrins whose structures had been determined. However, $2F_o - F_c$ and $F_o - F_c$ difference maps revealed that there was extra electron density that the model did not account for, as shown in Figure 3. In particular, there were three regions of additional electron density that were present in $F_o - F_c$ omit maps: (i) a region that bulged out of the carbonate density, (ii) a region that resembled an arginyl side chain, and (iii) regions of spherical density that resembled water molecules (Figure 3, left panel). However, it was not possible to build other anions (such as oxalate) into the carbonate density or additional solvent molecules because of disallowed close contacts with other atoms at the iron-binding site. After extensive model building, the additional density could be accounted for by the introduction of two alternative conformations of the side chain of Arg-124, the carbonate anion, and some water molecules, as shown in Figure 4. Refinement showed that the same phenomenon was present in both crystal forms; when the occupancies were refined with SHELXL (see earlier), the orthorhombic form had occupancies of 0.63 and 0.37 for the A and B conformations, respectively, whereas these values in the tetragonal form were 0.65 and 0.35, respectively. Additional evidence in support of these two conformations is given in Figure 3 (right panel), which represents an $F_o - F_c$ map with the atoms of the A conformer omitted and the atoms of the B conformer present at an occupancy of 0.35; additional electron density is again present, corresponding to the positions of the atoms (and additional water molecules) of the A conformation.

The A conformations of Arg-124 and the carbonate correspond to the positions of these atoms in other lactoferrins and transferrins for which structures have been

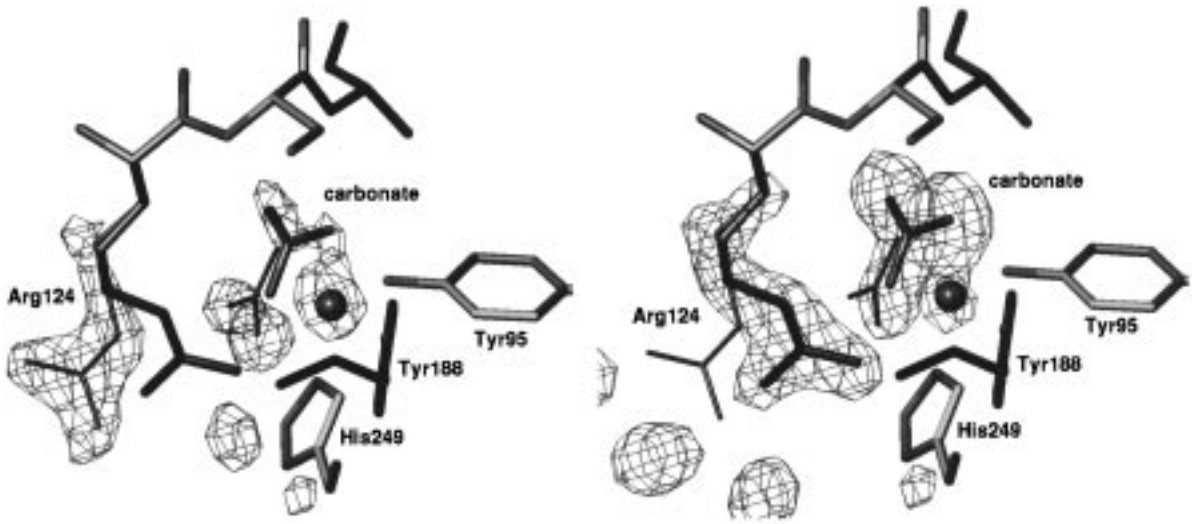

FIGURE 3: Difference electron density maps of the iron-binding site for the A and B conformers of the tetragonal crystal form of hTF/2N. The iron atom is represented by a red sphere; residues involved in the iron-binding site are labeled together with the carbonate anion. For Arg-124 and the carbonate, atoms in the A conformation are represented by the thick cylinders; these atoms in the B conformation are represented by the thin cylinders. In the left panel is an $F_o - F_c$ difference map contoured at 3σ. The map was calculated after omitting the atoms corresponding to the B conformer of Arg-124, the carbonate, and WAT-699 and with the corresponding atoms in the A conformer set to an occupancy of 0.65. In the right panel is an $F_o - F_c$ difference map contoured at 3σ. The map was calculated after omitting the atoms corresponding to the A conformer of Arg-124, the carbonate, and WAT-700, -701, and -702, and with the corresponding atoms in the B conformer set to an occupancy of 0.35. In each figure, electron density corresponding to the omitted atoms can be seen; see the text for details.

determined. The A conformations of both crystal forms are shown in Figure 4 (panel A, orthorhombic form; and panel C, tetragonal form), and the geometries of the resulting iron-binding sites are given in Table 5. This A conformation is assumed to correspond to the high-pH binding site geometry for human transferrin. In this conformation, the iron coordination is distorted octahedral with bond angle deviations of up to 20° from ideal octahedral geometry. The carbonate ion is bound in a slightly asymmetric bidentate fashion to the iron; in both crystal forms, the shorter of the two Fe(III)−O (CRB) bonds is that which is trans to His-249, and for which the bond angle with the trans ligand is closest to the ideal 180° [O1 (CRB)−Fe(III)−NE2 (His-249) = 168° for crystal form I and 170° for crystal form II]. In the A conformation, the Arg-124 side chain is folded around the carbonate ion such that both the NE and NH2 atoms of Arg-124 are hydrogen bonded to the carbonate O2 atom [N−O bond distances of 2.81 and 2.74 Å (crystal form I) and 2.57 and 2.60 Å (crystal from II)]. The carbonate oxygen atoms also receive hydrogen bonds from Thr-120 OG1, and the main chain amide nitrogen atoms of Ala-126 and Gly-127, at the N terminus of the helix involving residues 124−136 [helix 5 in the standard notation (*1*)]. In the tetragonal crystal form, this conformation is also associated with three well-defined water molecules (WAT-700, -701, and -702) which are hydrogen bonded to the Arg-124 side chain.

In the B conformations [Figure 4, panel B (orthorhombic form) and panel D (tetragonal form)], the side chain of Arg-124 is more extended and has moved away from the iron-binding site. This motion is mostly around the side chain torsion angle χ_3. For this side chain, χ_2 changes from 177 to 167° and from 177 to 173° while χ_3 changes from 52 to 153° and from 51 to 108° in crystal forms I and II, respectively. As shown in Figure 4 (panels B and D), the extended Arg-124 side chain takes up a slightly different conformation in the two crystal forms. In each crystal form, the carbonate ion is still bidentate, but is more asymmetrically bound with ligand bond distances of 1.99 and 2.42 Å (crystal form I) and 2.03 and 2.46 Å (crystal form II). Most notably, the carbonate has rotated some 30° around the iron atom such that the O2 atom is much more directly trans to Tyr-95 [O2 (CRB)−Fe(III)−OH (Tyr-95) = 169−171° compared with 155° in the A conformation], and the O1 atom is no longer directly trans to His-249 [O1 (CRB)−Fe(III)−NE2 (His-249) = 142 and 133° for the two crystal forms]. Again, the shorter of the two Fe(III)−O bonds is that which is most directly trans to another ligand [Fe(III)−O1 (CRB) = 1.99 and 2.03 Å for the two crystal forms]. It should be noted that, for both crystal forms, the trans oxygen is O1 in conformer A and O2 in conformer B; this is the result of the 30° rotation of the carbonate about the iron atom. The most significant feature of the B conformation is that the hydrogen bonding of the carbonate ion has been substantially disrupted; the carbonate has moved away from the helix 5 N terminus such that both the O1 (CRB)···NH (Ala-126) and the O3 (CRB)···NH (Gly-127) hydrogen bonds are lost. In the orthorhombic crystal form, both of the hydrogen bonds between the carbonate and the Arg-124 side chain are lost (Figure 4B); however, because the movement of the Arg-124 side chain is less in the tetragonal crystal form, a hydrogen bond is retained between the O3 atom of the carbonate and the NE atom of Arg-124 (Figure 4D). In the tetragonal crystal form, the water molecules WAT-700, -701, and -702 are absent, but a new water molecule (WAT-699) appears and has a low crystallographic *B*-factor of 7.1 Å^2; WAT-699 appears to stabilize the B conformation of the carbonate by forming hydrogen bonds with the O1 (hydrogen bond length = 2.79 Å) and O3 (2.97 Å) atoms of the carbonate and with WAT-542 (2.70 Å) and WAT-544 (2.77 Å).

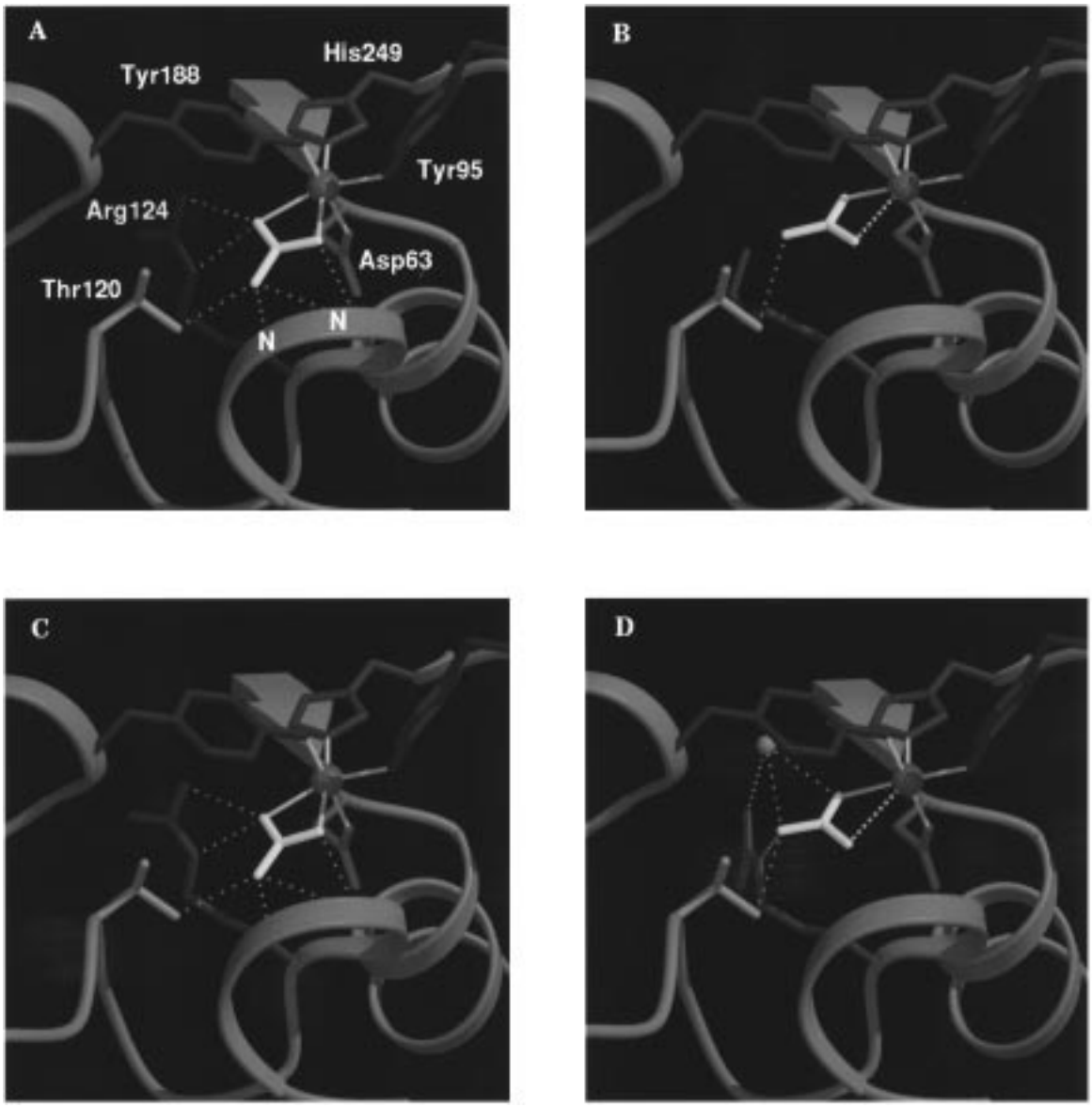

FIGURE 4: Structures of the alternative conformations of the iron-binding sites in two different crystal forms of hTF/2N: (A) orthorhombic crystal form of conformer A, (B) orthorhombic crystal form of conformer B, (C) tetragonal crystal form of conformer A, and (D) tetragonal crystal form of conformer B. The iron atom is indicated by the red sphere and the carbonate by the white triangular structure. Ligands to the iron from Asp-63, Tyr-95, Tyr-188, His-249, and the carbonate anion are indicated by thin white cylinders. Hydrogen bonds are indicated by dashed white lines. The side chain for Thr-120 is included; other side chains and water molecules have been omitted to simplify the figure. The main chain amide nitrogen atoms of Ala-126 and Gly-127 are indicated by N. The figure was generated using the programs Molscript (*58*) and Raster3D (*59*).

Functional Implications of the Alternative Conformations of Fe−hTF/2N. The disorder at the iron-binding site of hTF/2N is restricted to the carbonate anion, the side chain of Arg-124, and four water molecules (WAT-699, -700, -701, and -702). In contrast, the electron density maps of the side chains of Lys-206 and Lys-296 suggest that these residues are highly ordered (average *B* values of the side chain atoms are 13.6 and 15.1 Å^2, respectively). The clear definition of these lysine residues suggests that the observed structural changes at the iron-binding site occur prior to any movement of either side chain in the dilysine trigger model. In addition, the changes at the iron-binding site are highly localized; there is no evidence of conformational heterogeneity in other side chains adjacent to Arg-124.

The high quality of the diffraction data obtained for crystal forms I and II implies an absence of significant heterogeneity in the overall structures or their packing. The occurrence of related positional disorder at the metal-binding sites in both crystal forms (with very different crystal packing) argues against any contribution from the crystal packing or crystallization components to the observed disorder. Alternative conformations at the iron-binding site have not been observed with other transferrins or lactoferrins whose crystal structures have been determined. There are several possible explanations for this. First, the other structures have been determined at lower resolution than the hTF/2N structures reported here (see Table 1). At lower resolution, evidence for alternative conformations of groups of atoms may be less conclusive. Second, several of the structures have been determined at pH values substantially greater than pH 6.0; as such, the iron-bound forms of the molecules would be stable, and only the high-pH conformations would be expected. Third, many of the iron-release studies have been performed only with human transferrin or human lactoferrin;

Table 5: Geometry of the Iron-Binding Site for Several Transferrins

(A) Bond Distances at the Iron-Binding Site (Å)

	hTF/2N[a] ($P2_12_12_1$)	hTF/2N[a] ($P4_12_12$)	hLF/2N[b]	oTF/2N[c]
Fe(III)−OD1 (Asp-63)	2.02	2.03	1.99	2.2
Fe(III)−OH (Tyr-95)	1.99	1.97	2.00	1.8
Fe(III)−OH (Tyr-188)	1.90	1.88	1.92	2.0
Fe(III)−NE2 (His-249)	2.10	2.04	2.15	2.1
Fe(III)−O1 (CRB)[d]	2.06	2.08	2.09	1.9
Fe(III)−O2 (CRB)[d]	2.24	2.19	2.23	2.1

(B) Bond Distances (Å) and Angles (deg) for the Carbonate Anion in hTF/2N[a]

	A conformation		B conformation	
	form I ($P2_12_12_1$)	form II ($P4_12_12$)	form I ($P2_12_12_1$)	form II ($P4_12_12$)
O1 (CRB)−Fe(III)	2.06	2.08	2.42	2.46
O2 (CRB)−Fe(III)	2.24	2.19	1.99	2.03
O1 (CRB)−Fe(III)−NE2 (His-249)	168	171	142	133
O2 (CRB)−Fe(III)−OH (Tyr-95)	155	155	171	169
O1 (CRB)−NH (Ala-126)	3.02	2.83	3.81	3.72
O2 (CRB)−NE (Arg-124)	2.81	2.74	5.59	3.91
O2 (CRB)−NH2 (Arg-124)	2.57	2.60	7.11	4.57
O3 (CRB)−NE (Arg-124)	3.41	3.50	4.61	2.98
O3 (CRB)−NH (Gly-127)	2.97	2.83	5.35	5.28
O3 (CRB)−OG1 (Thr-120)	2.63	2.71	3.22	3.17

[a] This study. [b] Taken from ref *55*. [c] Taken from ref *11*. [d] A conformation of hTF/2N.

thus, it is possible that other transferrins retain their iron to a lower pH than the well-characterized sites of human transferrin. In this connection, we note that full-length transferrin was crystallized at pH 6.3 and that, when the crystal structure was determined (*51*), the molecules in the crystal were found to have iron bound only in their C-lobe sites; iron had been released from the N-lobe which had assumed its fully open conformation. Last, the iron-release properties of the isolated N-lobe may be different from the those of the full-length molecule where the presence of the C-lobe may have an influence.

It is possible that the B conformation of hTF/2N represents a crystallographically stable intermediate that results from the protonation of the carbonate. In this model for iron release from hTF/2N, the initial step is protonation of the carbonate anion, resulting in bicarbonate. The reduction in charge on the anion results in movement of the bicarbonate anion away from the iron site in such a way that it becomes detached from the helix 5 N terminus. Exactly the same type of movement of the anion is found for two mutants of hLF/2N in which the anion-binding arginine side chain has been mutated (R121S and R121E mutants), and in which iron binding is destabilized (*52*). Concomitant with this anion movement is the displacement of water molecules 700, 701, and 702. Disruption of the stabilizing hydrogen bonding network involving these water molecules allows the movement of the side chain of Arg-124 to a position where the bicarbonate anion is now stabilized through hydrogen bonding involving the NE atom of Arg-124 and water molecule 699. The net result of this conformational change is the partial removal of the anion from the metal and a substantial weakening of the hydrogen bonding between the anion and the protein. This would result in a substantial reduction in the binding affinity between metal, anion, and protein in a manner similar to that which occurs for the lactoferrin mutants (*52*).

In the dilysine trigger model, the next step would be protonation of either Lys-206 or Lys-296 followed by cleft opening which allows release of the anion. The cleft opening with associated physical removal of further metal ligands would allow the release of the iron, presumably to a competitive chelator. This iron-release model for hTF/2N is similar to mechanism IV of El Hage Chahine and Pakdaman (*26*) in which carbonate protonation and loss (*53*) is followed by slow protonation of the protein ligands with subsequent release of the metal. Other studies have also demonstrated that the side chain for Arg-124 is flexible and capable of movement. The crystal structure of human copper−lactoferrin at 2.1 Å showed that the metal-binding sites in the N- and C-lobes are different (*54*); whereas the C-lobe site is distorted octahedral with an asymmetrically bidentate anion, the N-lobe site is square pyramidal with a monodentate anion. These changes are accommodated in the structure by small movements of the metal ion, anion, and Arg-124 side chain within each binding site without affecting the overall protein structure.

The crystal stuctures reported in this study suggest that there is a stable intermediate that may be involved in the release of iron from hTF/2N. The changes caused by the formation of this intermediate should be able to be detected by NMR. Such studies are the focus of our ongoing research program.

REFERENCES

1. Baker, E. N. (1994) *Adv. Inorg. Chem. 41*, 389−463.
2. Jamroz, R. C., Gasdaska, J. R., Bradfield, J. Y., and Law, J. H. (1993) *Proc. Natl. Acad. Sci. U.S.A. 90*, 1320−1324.
3. MacGillivray, R. T. A., Mendez, E., Shewale, J. G., Sinha, S. K., Lineback-Zins, J., and Brew, K. (1983) *J. Biol. Chem. 258*, 3543−3553.
4. Welch, S. (1990) *Comp. Biochem. Physiol. B97*, 417−428.
5. Baldwin, G. S. (1993) *Comp. Biochem. Physiol. B106*, 203−218.
6. Park, I., Schaeffer, E., Sidoli, A., Baralle, F. E., Cohen, G. N., and Zakin, M. M. (1985) *Proc. Natl. Acad. Sci. U.S.A. 82*, 3149−3153.
7. Anderson, B. F., Baker, H. M., Dodson, E. J., Norris, G. E., Rumball, S. V., Waters, J. M., and Baker, E. N. (1987) *Proc. Natl. Acad. Sci. U.S.A. 84*, 1769−1773.
8. Anderson, B. F., Baker, H. M., Norris, G. E., Rice, D. W., and Baker, E. N. (1989) *J. Mol. Biol. 209*, 711−734.
9. Haridas, M., Anderson, B. F., and Baker, E. N. (1995) *Acta Crystallogr. D51*, 629−646.
10. Bailey, S., Evans, R. W., Garratt, R. C., Gorinsky, B., Hasnain, S., Horsburgh, C., Jhoti, H., Lindley, P. F., Mydin, A., Sarra, R., and Watson, J. L. (1988) *Biochemistry 27*, 5804−5812.
11. Kurokawa, H., Mikami, B., and Hirose, M. (1995) *J. Mol. Biol. 254*, 196−207.
12. Rawas, A., Muirhead, H., and Williams, J. (1996) *Acta Crystallogr. D52*, 631−640.
13. Lindley, P. F., Bajaj, M., Evans, R. W., Garratt, R. C., Hasnain, S. S., Jhoti, H., Kuser, P., Neu, M., Patel, K., Sarrar, R., Strange, R., and Walton, A. (1993) *Acta Crystallogr. D49*, 292−304.
14. Moore, S. A., Anderson, B. F., Groom, C. R., Haridas, M., and Baker, E. N. (1997) *J. Mol. Biol. 274*, 222−236.
15. Anderson, B. F., Baker, H. M., Norris, G. E., Rumball, S. V., and Baker, E. (1990) *Nature 344*, 784−786.

16. Rawas, A., Muirhead, H., and Williams, J. (1997) *Acta Crystallogr. D53*, 464−468.
17. Grossmann, J. G., Neu, M., Pantos, E., Schwab, F. J., Evans, R. W., Townes-Andrews, E., Lindley, P. F., Appel, H., Thies, W. G., and Hasnain, S. S. (1992) *J. Mol. Biol. 225*, 811−819.
18. Klausner, R. D., Ashwell, J. V., VanRenswoude, J. B., Harford, J., and Bridges, K. (1983) *Proc. Natl. Acad. Sci. U.S.A. 80*, 2263−2267.
19. Ponka, P. (1997) *Blood 89*, 1−25.
20. Aisen, P., and Leibman, A. (1973) *Biochim. Biophys. Acta 304*, 797−804.
21. Egyed, A. (1973) *Biochim. Biophys. Acta 304*, 805−813.
22. Williams, S. C., and Woodworth, R. C. (1973) *J. Biol. Chem. 248*, 5848−5853.
23. Martinez-Medellin, J., and Schulman, H. M. (1973) *Biochem. Biophys. Res. Commun. 53*, 32−38.
24. Morgan, E. H. (1979) *Biochim. Biophys. Acta 580*, 312−326.
25. Nunez, M. T., Gaete, V., Abra-Watkins, J. A., and Glass, J. (1990) *J. Biol. Chem. 265*, 6688−6692.
26. El Hage Chahine, J.-M., and Pakdaman, R. (1995) *Eur. J. Biochem. 230*, 1102−1110.
27. Thompson, C. P., Grady, J. K., and Chasteen, N. D. (1986) *J. Biol. Chem. 261*, 13128−13134.
28. Bali, P. K., and Aisen, P. (1991) *Biochemistry 30*, 9947−9952.
29. Sipe, D. M., and Murphy, R. F. (1991) *J. Biol. Chem. 266*, 8002−8007.
30. Egan, T. J., Zak, O., and Aisen, P. (1993) *Biochemistry 32*, 8162−8167.
31. Dewan, J. C., Mikami, B., Hirose, M., and Sacchettini, J. C. (1993) *Biochemistry 32*, 11963−11968.
32. Funk, W. D., MacGillivray, R. T. A., Mason, A. B., Brown, S. A., and Woodworth, R. C. (1990) *Biochemistry 29*, 1654−1660.
33. Mason, A. B., Funk, W. D., MacGillivray, R. T. A., and Woodworth, R. C. (1991) *Protein Expression Purif. 2*, 214−220.
34. Woodworth, R. C., Mason, A. B., Funk, W. D., and MacGillivray, R. T. A. (1991) *Biochemistry 30*, 10824−10829.
35. Wang, Y., Chen, J., Luo, Y., Funk, W. D., Mason, A. B., Woodworth, R. C., MacGillivray, R. T. A., and Brayer, G. D. (1992) *J. Mol. Biol. 227*, 575−576.
36. Otwinowski, Z., and Minor, W. (1997) *Methods Enzymol. 276*, 307−326.
37. CCP4 (1994) *Acta Crystallogr. D50*, 760−763.
38. Yang, F., Lum, J. B., McGill, J. R., Moore, C. M., Naylor, S. L., van Bragt, P. H., Baldwin, W. D., and Bowman, B. H. (1984) *Proc. Natl. Acad. Sci. U.S.A. 81*, 2752−2756.
39. Brünger, A. T., Kuriyan, J., and Karplus, M. (1987) *Science 235*, 458−460.
40. Tronrud, D. E., Ten Eyck, L. F., and Matthews, B. W. (1987) *Acta Crystallogr. A43*, 489−501.
41. Tronrud, D. E. (1992) *Acta Crystallogr. A48*, 912−916.
42. Navaza, J., and Saludjian, P. (1997) *Methods Enzymol. 276*, 581−594.
43. Read, R. J. (1986) *Acta Crystallogr. A42*, 140−149.
44. Sheldrick, G. M. (1990) *Acta Crystallogr. A46*, 467−473.
45. Mason, A. B., Miller, M. K., Funk, W. D., Banfield, D. K., Savage, K. J., Oliver, R. W. A., Green, B. N., MacGillivray, R. T. A., and Woodworth, R. C. (1993) *Biochemistry 32*, 5472−5479.
46. Ramakrishnan, C., and Ramachandran, G. N. (1965) *Biophys. J. 5*, 909−933.
47. Matthews, B. W. (1972) *Macromolecules 5*, 818−819.
48. Diamond, R. (1992) *Protein Sci. 1*, 1279−1287.
49. Murphy, M. E. P., Lindley, P. F., and Adman, E. T. (1997) *Protein Sci. 6*, 761−770.
50. Schimo-Oka, T., Hagiwara, Y., and Ozawa, E. (1986) *J. Cell. Physiol. 126*, 341−351.
51. Zuccola, H. J. (1993) Ph.D. Thesis, Georgia Institute of Technology, Atlanta, GA.
52. Faber, H. R., Bland, T., Day, C. L., Norris, G. E., Tweedie, J. W., and Baker, E. N. (1996) *J. Mol. Biol. 256*, 352−363.
53. Kretchmar Nguyen, S. A., Craig, A., and Raymond, K. N. (1993) *J. Am. Chem. Soc. 115*, 6758−6764.
54. Smith, C. A., Anderson, B. F., Baker, H. M., and Baker, E. N. (1992) *Biochemistry 31*, 4527−4533.
55. Day, C. L., Anderson, B. F., Tweedie, J. W., and Baker, E. N. (1993) *J. Mol. Biol. 232*, 1084−1100.
56. McRee, D. E. (1992) *J. Mol. Graphics 10*, 44−46.
57. Laskowski, R. A., MacArthur, M. W., Moss, D. S., and Thornton, J. M. (1993) *J. Appl. Crystallogr. 26*, 283−291.
58. Kraulis, P. (1991) *J. Appl. Crystallogr. 24*, 946−950.

BI980355J